11

Dynamic Analysis of Laser Ablation of Biological Tissue by Optical Coherence Tomography

Masato Ohmi and Masamitsu Haruna
Course of Health Science, Graduate School of Medicine
Osaka University
Japan

1. Introduction

Laser ablation is widely used in optical material engineering but also in clinical medicine. Actually, it has been used for evaporation and cutting of biological tissue in surgical operations; for example, the refractive surgery of cornea (Trokel *et al.* 1983; Puliafito *et al.* 1985) and the surgery of vascular (Isner *et al.* 1987). In particular, various types of CW and pulsed lasers have been considered for removal of hard dental tissues. Laser ablation may potentially provide an effective method for removal of caries and hard dental tissues with minimal thermal and mechanical damage to surrounding tissue. An important issue is quantitatively determining the dependence of tooth ablation efficiency or the ablation rate on the laser parameters such as repetition rate and energy of laser pulses. Up to now, the measurement has been made by observation of the cross section of the tissue surface, using a microscope or SEM, after cutting and polishing of a tissue sample (Esenaliev *et al.* 1996). This sort of process is cumbersome and destructive. On the other hand, shape of the tissue surface may change gradually with time after irradiation of laser pulses. The deformation of tissue surface is due to dehydration. The surrounding tissue may also suffer serious damage from laser ablation if the laser fluence is too high. Therefore, in-situ observation of the cross section of tissue surface is strongly required.

A very promising candidate for such an in-situ observation is the so-called optical coherence tomography (OCT) (Huang *et al.* 1991). The OCT is a medical diagnostic imaging technology that permits in-situ, micron-scale, tomographic cross-sectional imaging of microstructures in biological tissues (Hee *et al.* 1995; Izatt *et al.* 1996; Brezinski *et al.* 1996). At present, in the practical OCT, a super luminescent diode (SLD) is used as the light source for the low-coherence interferometer, providing the spatial resolution of 10 to 20 μm along the depth. Therefore, the OCT is potential for monitoring of the surface change during tissue ablation with micrometer resolution. Boppart et al have first demonstrated OCT imaging for observation of *ex vivo* rat organ tissue (Boppart *et al.* 1999). Alfrado et al have demonstrated thermal and mechanical damage to dentin by sub-microsecond pulsed IR lasers using OCT imaging (Alfano *et al.* 2004). We have also demonstrated an effective method for the *in situ* observation of laser ablation of biological tissues based on OCT (Haruna *et al.* 2001; Ohmi *et*

al. 2005; Ohmi *et al.* 2007). In the traditional OCT system using a super-luminescent diode as a light source, imaging speed is limited. In fact, our first reported laser-ablation system, a time-domain OCT (TD-OCT) at the center wavelength of 0.8-μm is combined with a laser ablation system, where the optical axis of OCT is aligned with the 1.06-μm Q-switched YAG laser beam using a dichroic mirror. In this system, the data acquisition of each OCT image takes four seconds. The tissue laser ablation and the OCT imaging are repeated in turn. In this system, with this time delay for data acquisition, it is impossible to observe deformation of a crater and damage to the surrounding tissue due to thermal accumulation effects.
On the other hand, the recent application of Fourier-domain techniques with high-repetition rate swept laser source to OCT has led to an improvement in sensitivity of several orders of magnitude, toward high-speed OCT imaging (Yun *et al.* 2003; de Bore *et al.* 2003). Recently, we demonstrated true real-time OCT imaging of tissue laser ablation. A swept source OCT (SS-OCT) with 25 frames / s is used for the *in situ* observation, while tissue laser ablation is made continuously by 10-Hz YAG laser pulses (Ohmi *et al.* 2010). With this system, dynamic analysis of laser ablation can be achieved, taking thermal accumulation effects into account.
In this chapter, we summarize overview of *in situ* observation of biological tissue in laser ablation using OCT imaging technique. At first, laser ablation system with the time-domain OCT (TD-OCT) including the experimental data is described. Next, real-time *in situ* imaging of tissue ablation using swept source OCT (SS-OCT) is described. Laser ablation of hard and soft tissues including the ablation rate are demonstrated. Furthermore, the 3-D OCT image of the crater of biological tissue can be constructed by volume rendering of several hundred B-mode OCT images.

2. In-situ observation of laser ablation of biological tissue by time-domain OCT

2.1 System configuration

In order to achieve in-situ tomographic observation of the crater surface just after laser ablation of biological tissue, the laser-ablation optics and OCT imaging optics are combined. The system configuration is shown in **Fig. 1**. In laser ablation of tissue, the Q-switched Nd:YAG laser is used as the light source, which supplies laser pulses of 10 ns at the wavelength of 1.06 μm with the repetition rate of 10 Hz. The laser pulse is focused on a tissue sample via an x 10 objective with a 20-mm focal length lens. The focused beam spot size of 20 μm in the focal plane with the length of the beam waist is calculated of 630 μm. The laser pulse energy is typically 6.4 mJ with the energy per unit area of 5.1×10^3 J / cm^2 on the tissue surface.
On the other hand, the OCT system is a time-domain OCT (TD-OCT) which consists of the optical-fiber interferometer with the fiber-optic PZT phase modulators (Bouma *et al.* 2002). The light source is a 1.3-μm SLD whose output light of 13mW is coupled into a single-mode fiber directional coupler. For optical delay scanning, two identical fiber-optic PZT modulators are places on both reference and signal arms. In each PZT modulators, a nearly 20-m long single-mode fiber was wrapped around a cylindrical piezoelectric transducer. Two PZT modulators were driven in push-pull operation. The scanning depth along the optical axis becomes 1.0 mm when a 250-V triangular voltage is applied to two PZTs. In the sample arm of the interferometer, the collimated light beam of 6 mm diameter is focused on

a sample via a microscope. Fortunately, it is a common knowledge that zero dispersion of a silica fiber lies near 1.3 μm. A great advantage of the all-optical-fiber OCT of Fig. 1, therefore, is that the coherence length does not increase significantly even if there is a remarkable optical path difference between reference and signal arms. In fact, we measured the coherence length of 19.1 μm. This value was very close to the expected value of 18.2 μm from the spectral bandwidth of the SLD itself. This value determines the resolution of OCT image along the optical axis. On the other hand, the lateral resolution is 5.6 μm determined by the focusing spot size of the x 10 objective used in the experiment. This value determines the resolution of OCT image along the optical axis.

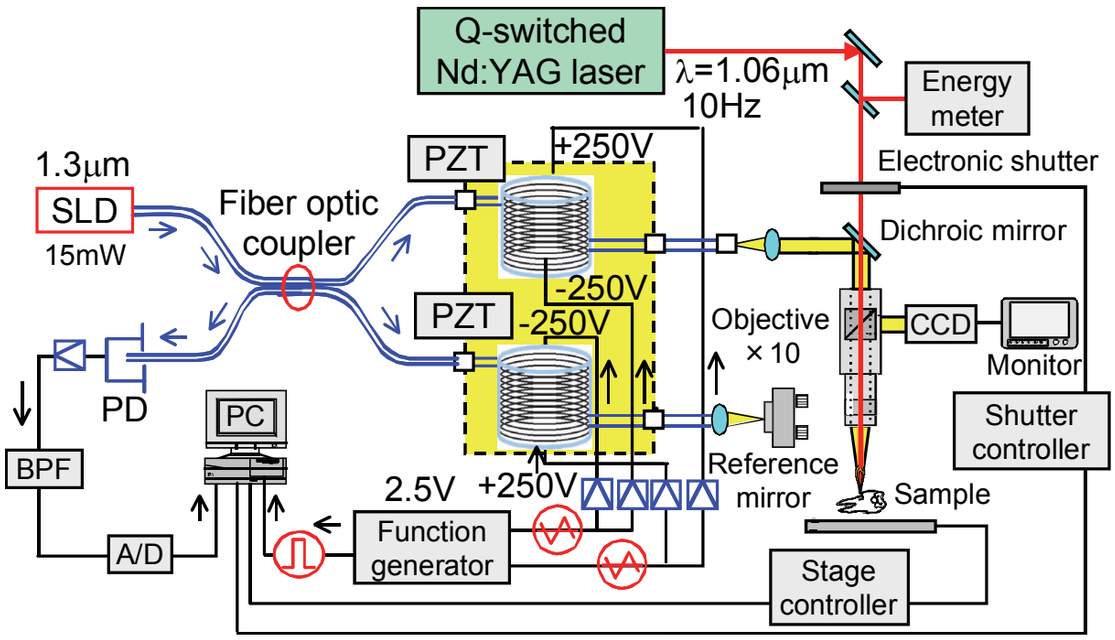

Fig. 1. System configuration of laser ablation with the time-domaion OCT (TD-OCT).

A key point for in-situ observation of the crater surface is that the YAG laser beam is aligned with the SLD light beam on the sample arm of the interferometer. These two light beams are combined or divided by a dichroic mirror, and an electronic shutter is placed in front of the YAG laser. Therefore, both the YAG laser and SLD light illuminate the same point on the tissue sample. In the experiment, at first, a certain number of YAG laser pulses are irradiated on the tissue sample, and a crater is formed on the sample surface. The YAG laser beam is then cut off with the electronic shutter, followed by obtaining an OCT image of the crater. The OCT imaging takes one second in the case where the image size is 1.0 x 1.0 mm^2 with a pixel size of 2.5 x 2.5 μm^2. After the OCT imaging, the laser ablation is again started with

irradiation of a certain number of laser pulses. The laser ablation and OCT imaging are repeated by turn. This process is automatically controlled in our system. The characteristic of the system performance is summarized in Table 1, where the repletion rate of PZT phase modulator is 200 Hz at the OCT imaging area of 1 x 1 mm^2.

2.2 In-situ observation of ablation crater and the evaluation of ablation rate

In the experiment, human tooth enamel was used for the sample of laser ablation. A human tooth is a suitable representative for a hard tissue sample, because the tooth consists of two layers, enamel and dentine, and there is a remarkable difference in refractive index and hardness between these two materials. The interface between enamel and dentine is therefore recognized clearly in the OCT image. The ablation rate is quite different for enamel and dentine, as will be discussed later. The crater shape is also different between enamel and dentine because of the abrupt change in hardness at the interface.The Nd:YAG laser pulses were focused on the surface of human tooth enamel to make the ablation crater depending upon the laser-pulse shot number. **Figure 2** shows a series of OCT images of craters of human tooth enamel, where N is the laser-pulse shot number. From these OCT images, surface change of the ablation crater of the human tooth enamel is clearly observed. Moreover, showing all of OCT images continuously, time-serial tomographic observation of the crater in laser ablation is carried out.

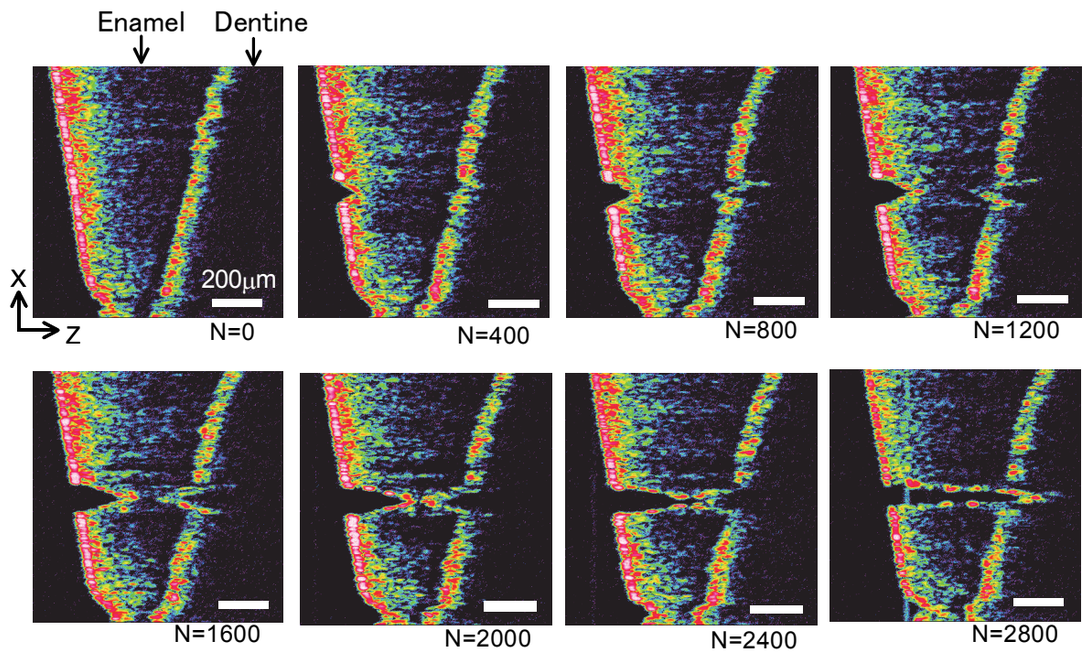

Fig. 2. A series of TD-OCT images of craters in laser ablation of human tooth.

The crater depth is also measured by the raster-scan signal of each OCT image. The measurement accuracy of the crater depth is 2.5 μm, which is determined by a pixel size of the OCT image. This value is smaller than the coherence length of 19μm of the SLD light source. The measured crater depths are plotted with respect to the laser-pulse shot number N, as shown in **Fig. 3**. From the data of N = 0 to 2000, a straight line was determined by the least squares method. The slope of the straight line yields the ablation rate of 0.11 μm / pulse with a standard deviation σ of 0.008 μm / pulse when the laser pulse energy is 16.0 mJ. Furthermore, from the data of N = 2200 to 2800, a straight line was determined by the least squares method. The slope of the straight line yields the ablation rate of 0.46 μm / pulse with a standard deviation σ of 0.015 μm / pulse in the human tooth dentine. The ablation rate of human tooth dentine is almost four times larger than human tooth enamel. Dentine is somewhat soft tissue rather than human tooth enamel. From the experimental results described above, one can find that OCT is really useful for monitor of the crater shape and the ablation rate with the damage of the surrounding tissues.

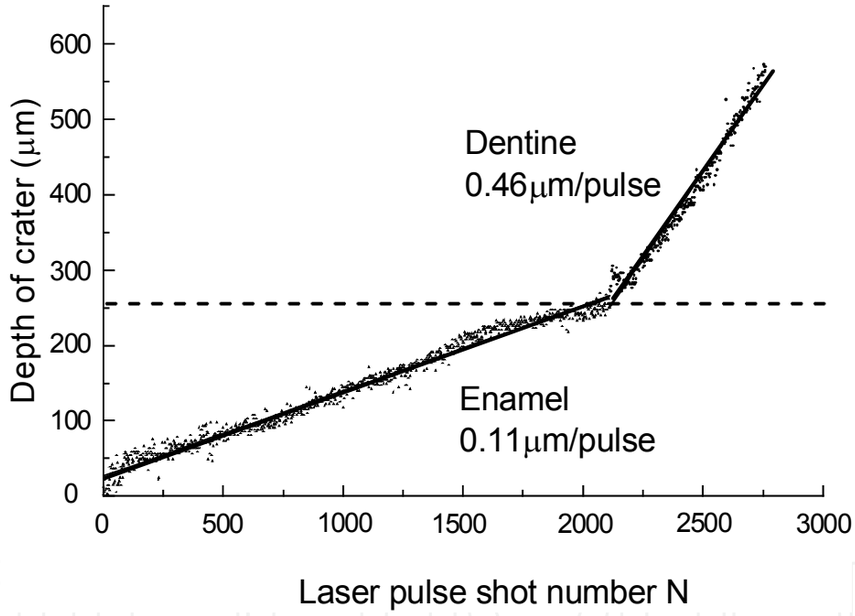

Fig. 3. Measurement of ablation rate of human tooth.

3. Real-time imaging of laser ablation of biological tissue by swept-source OCT

3.1 System configuration

In the former system, with this time delay for data acquisition, it is impossible to observe deformation of a crater and damage to the surrounding tissue due to thermal accumulation effects. In order to perform dynamic analysis of laser ablation of biological tissue, a swept-source OCT (SS-OCT) is combined with a YAG-laser ablation system, as shown in **Fig. 4**. In the SS-OCT, the optical source is an extended-cavity semiconductor wavelength-swept laser

employing an intracavity polygon scanner filter (HSL-2000, santec corporation). The lasing frequency is swept linearly with time, to obtain the reflected light distribution along the depth of the tissue sample. Fourier transformation of the interference signals results in reflected light distribution along the tissue depth. The SS-OCT consists of fiber-optic components, and the illuminating laser beam on the signal arm of the OCT interferometer is aligned with the YAG laser beam using a dichroic mirror. The light reflected from the reference mirror and the sample were recieved through magneto-optic circulators and combined by a 50/50 coupler. A fiber-optic polarization controller in the reference arm and the sample arm were used to align the polarization states of the two arms. The laser beam is then scanned with a Galvano mirror, resulting in a clear image of the ablation crater of the tissue sample. The center wavelength of the swept laser is 1.33 μm, with a wavelength scanning range of 110 nm. The sweep frequency of the laser source is 20 kHz at 25 frames / s, while the imaging area is 1 x 1 mm^2 with a pixel size of 8 x 5 μm. The real-time imaging of tissue laser ablation is thus realized in a fusion system of YAG-laser ablation and the fiber-optic SS-OCT. The measured coherence length of the SS-OCT system is 13 μm.

An electronic shutter is placed in front of the dichroic mirror to exactly adjust the ablation time. Both the YAG laser beam and the OCT probing laser beam are focused with the x 10 objective. The focused spot size is adequately adjusted by the laser beam width. In the experiment, the focused beam spot size is nearly 20 μm on the tissue surface. On the other hand, the focused spot size of the OCT probing beam is 5.6 μm, with a focal depth of only 40 μm. The out-of-focusing is unavoidable in the resulting OCT images, because there is no focus tracking mechanism in the present system.

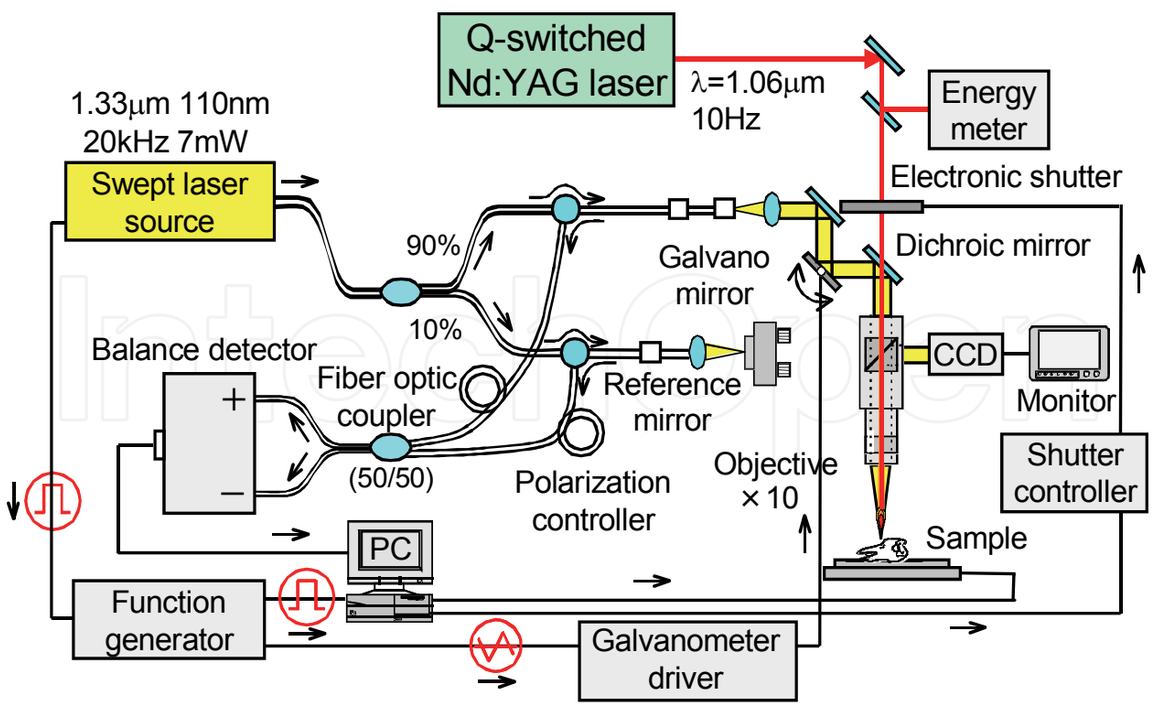

Fig. 4. System configuration of laser ablation with the swept-source OCT (SS-OCT).

3.2 Real-time imaging of tissue laser ablation and the evaluation of ablation rate

3.2.1 Hard tissue ablation

In the experiment, the laser pulse energy is typically 15.7 mJ with the energy per unit area of 5.0 x 10^3 J / cm^2 with a focused beam spot size of 20 μm on the tissue surface. The laser ablation of a human tooth made is continuously by the Q-switched YAG laser. Time-sequential OCT images of the crater of a human tooth are shown, where N is the shot number of the illuminating laser pulses, as shown in **Fig. 5**. The interface between enamel and dentine is clearly recognized in each OCT image because of the large refractive index difference between enamel (n = 1.652) and dentine (n = 1.546) (Ohmi *et al.* 2000). The crater depth increases gradually in the enamel, and it appears as if the interface between enamel and dentine juts out into the enamel. Near N = 2400, the YAG laser beam penetrates into the dentine through the enamel. The crater width becomes abruptly narrower in the dentine, reflecting the large difference in hardness between enamel and dentine. In addition, in the real-time imaging shown in **Fig. 5**, a small flying particle (debris), is observed in the crater, as indicated by a white circle, although the ablation plume is not imaged by OCT. The crater depth is measured in each OCT image, obtained by real-time imaging at 25 frames / s, where d is determined by the raster scan signal along the center of the crater. All measured values of d are plotted with respect to the shot number N of laser pulses, as shown in **Fig. 6**.

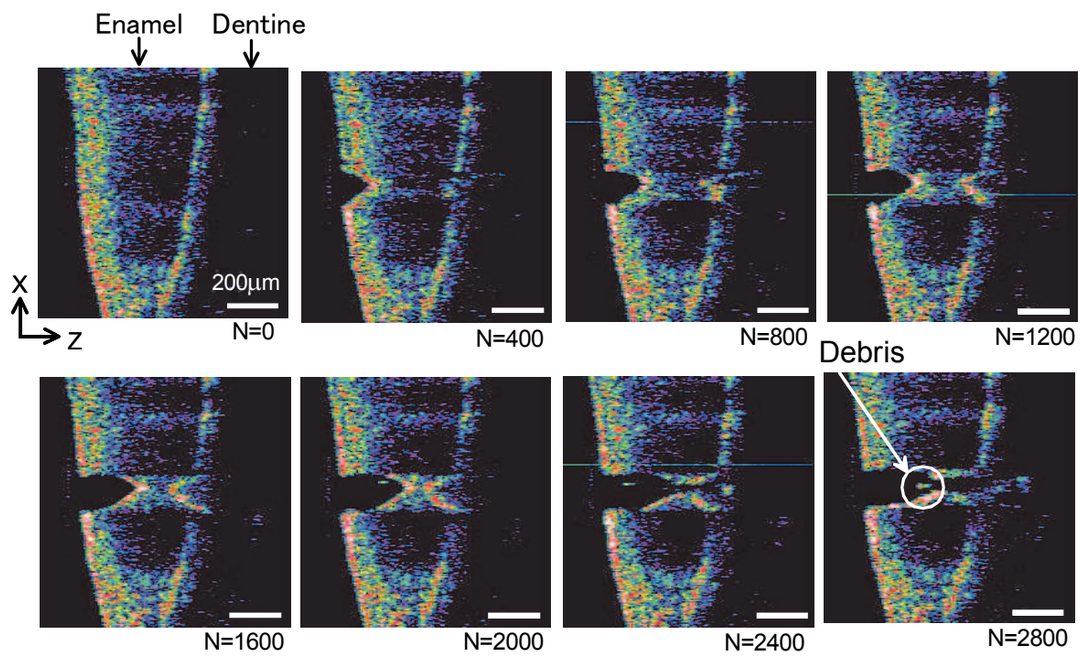

Fig. 5. A series of SS-OCT images of craters in laser ablation of human tooth.

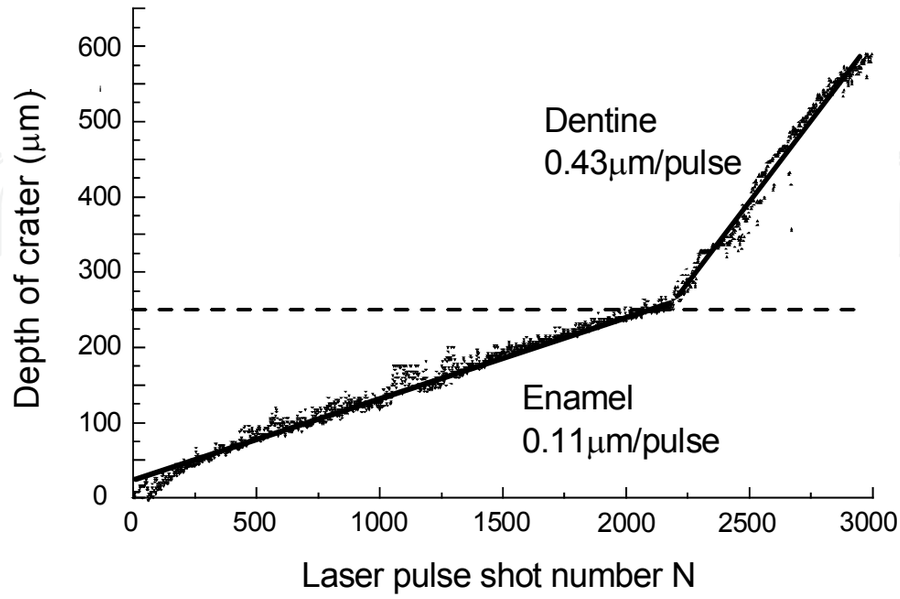

Fig. 6. Measurement of ablation rate of human tooth.

Furthermore, OCT images of craters formed after illuminating laser pulses in enamel and dentine are shown in **Fig. 7 (a)**, where the input laser fluence was 1.42 x 10^3 J / cm^2 to 6.87 x 10^3 J / cm^2. The ablation rate versus the input laser fluence for enamel and for dentine is also shown in **Fig. 7 (b)**. The ablation rate does not increase in linear proportion to the laser fluence, due to thermal accumulation effects, and it tends to saturate as the fluence increases. From the OCT image of the crater, the ablation volume of the crater increases according to the input laser fluence.

It is important to pay attention to the ablation rate and the volume of the crater. The ablation volume of a crater is evaluated in the following manner. In each frame of time-sequential OCT images, the crater is cut into 5-μm thick disks along the depth, under the assumption that the crater has a circular cross section. This assumption is consistent with the actual crater shape found in the 3-Dimensional OCT (3-D OCT) image of a human tooth, as will be shown later. The diameter is easily measured for each disk in the OCT image, and the crater volume is then counted by piling up 5-μm thick disks along the depth. All measured values of the ablation volume are plotted with respect to the shot number N of laser pulses, as shown in **Fig. 8**. From the slope of the straight line, the volume ablation rate of enamel and of dentine are obtained to be 1.31 x 10^4 μm^3 / pulse and 4.90 x 10^4 μm^3 / pulse, respectively. The volume ablation rate versus input laser fluence for enamel and for dentine is shown in **Fig. 9**. The volume ablation rate increases in linear proportion to the input laser fluence.

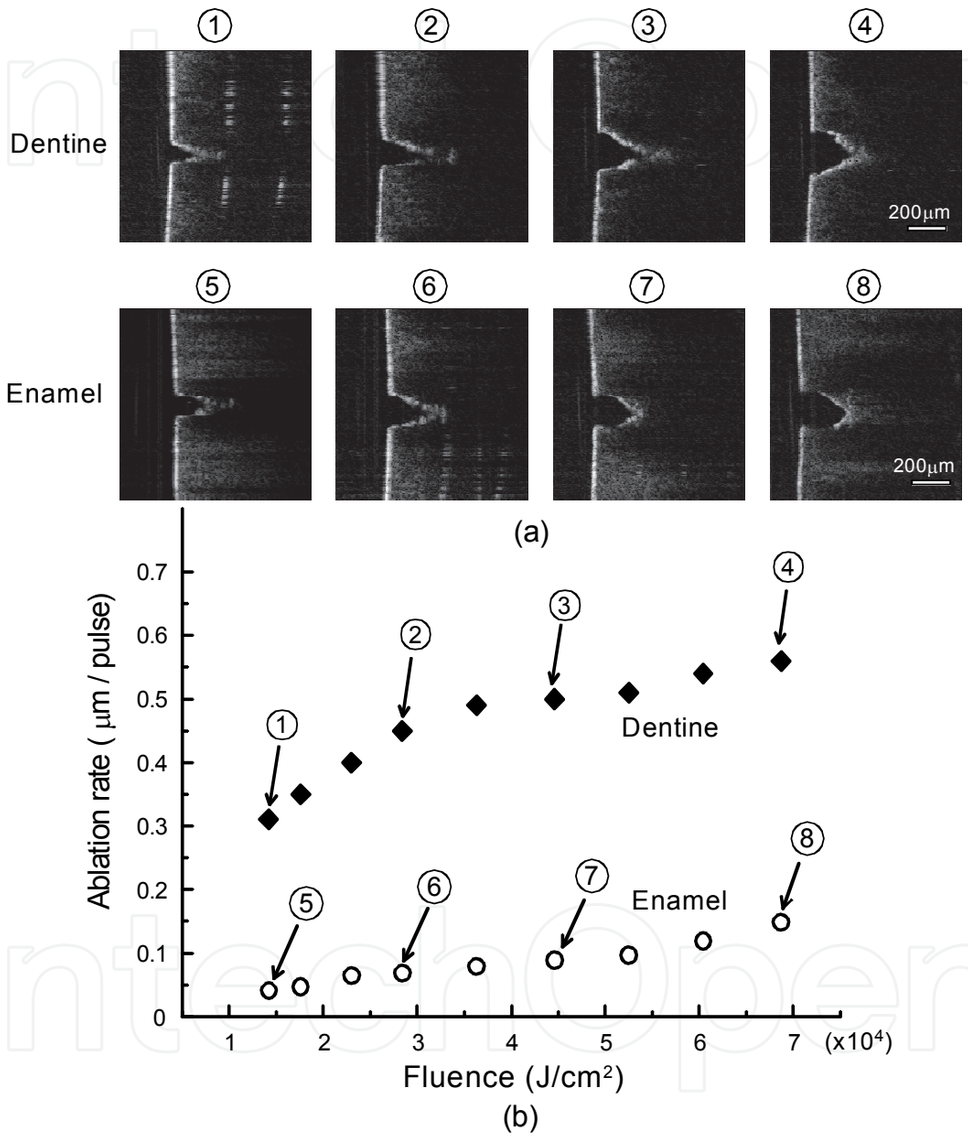

Fig. 7. Ablation rate versus laser fluence. (a) OCT images of the crater of enamel and dentine. (b) Ablation rate versus laser fluence.

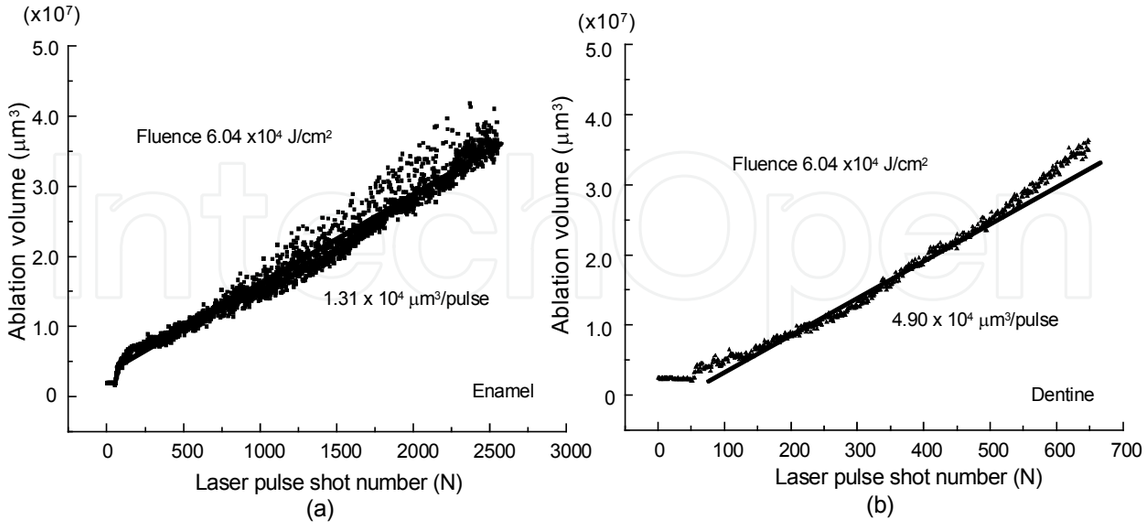

Fig. 8. Measured ablation volume versus laser shot number. (a) Enamel, (b) Dentine.

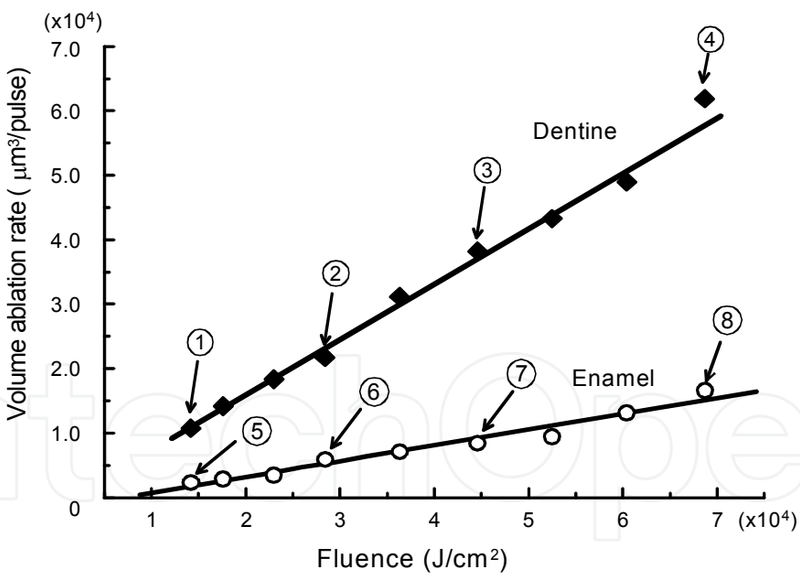

Fig. 9. Volume ablation rate versus laser fluence.

3.2.2 Soft tissue ablation

The aorta of a dog was used as an example of a soft tissue. An aorta has a three-layer wall that consists of the tunica intima, tunica media, and tunica adventitia. In the experiment, the YAG laser beam is focused on the inner surface of the aorta. In addition, the input laser fluence is reduced to 6.0 x 10^2 J / cm^2 to avoid the pronounced thermal accumulation effect

that occurs in soft tissue ablation. Time-sequential OCT images of the dog aorta are shown, where the shot number N of laser pulses is 0 to 50, as shown in **Fig. 10**. In particular, thermal deformation of the crater is found where upheaval and removal of tissues are observed, when N is larger than 10. The crater diameter on the tissue surface increases with N, and is widened to nearly 260 μm due to the thermal deformation. The ablation rate of the aorta is 16.2 μm / pulse with a standard deviation σ of 0.41 μm / pulse. In comparison to the hard tissue ablation described in the **Section 3.2.1**, the ablation rate of the aorta is nearly 150 times larger than that for the human tooth, even though the input laser fluence is only one tenth. On the other hand, in the case where the input laser fluence is reduced to 6.0 x 10^2 J / cm^2, the thermal deformation of the crater is suppressed, resulting in a narrower crater, 600 μm deep with a diameter of 35 μm, without any damage to the surrounding tissues.

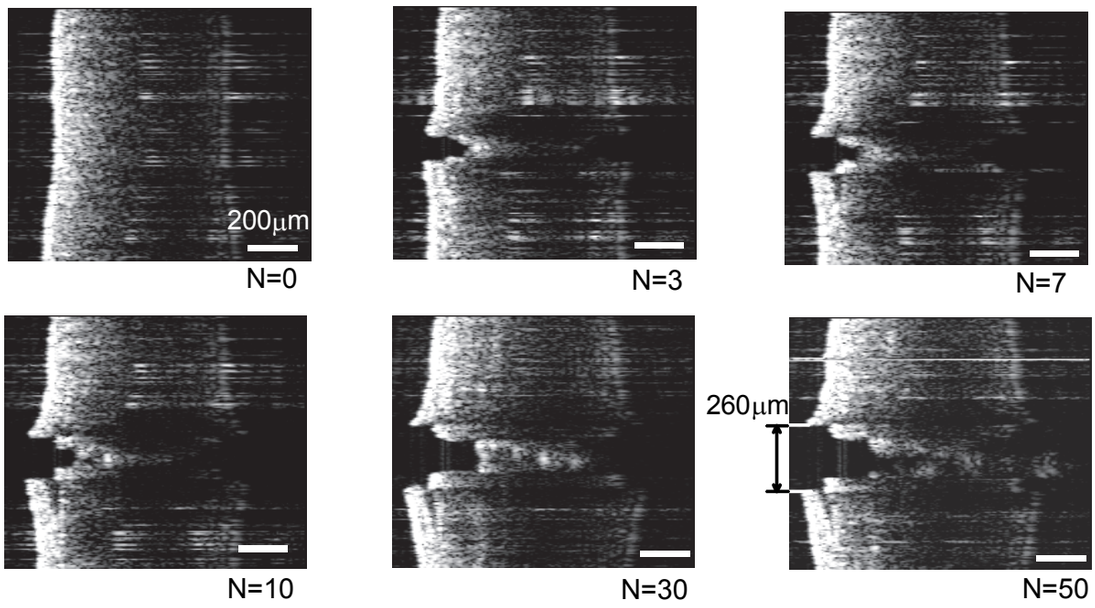

Fig. 10. Time-sequential OCT images of craters in laser ablation of dog aorta.

The 3-D OCT image of the crater of the aorta can be constructed by volume rendering of two hundred B-mode OCT images, obtained with a step of 5 μm over the distance of 0.5 mm, as shown in **Fig. 11 (a)**. The crater shape can be precisely observed in the 3-D OCT image. Under the condition where the input laser fluence is as large as 6.0 x 10^2 J / cm^2, smooth muscle fibers of the aorta surrounding the crater are coagulated and shrunken due to the thermal accumulation effect. As a result, the crater is expanded along the direction of the muscle fibers. The real-time OCT imaging is thus very useful for monitoring the thermal damage caused during soft tissue ablation. The 3-D OCT image of the crater of the human tooth is shown in **Fig. 11 (b)**. One can see that the crater of the human tooth has a circular cross section. This result is consistent with an assumption of the calculation of the ablation volume, as shown in **Figs. 8** and **Fig. 9**.

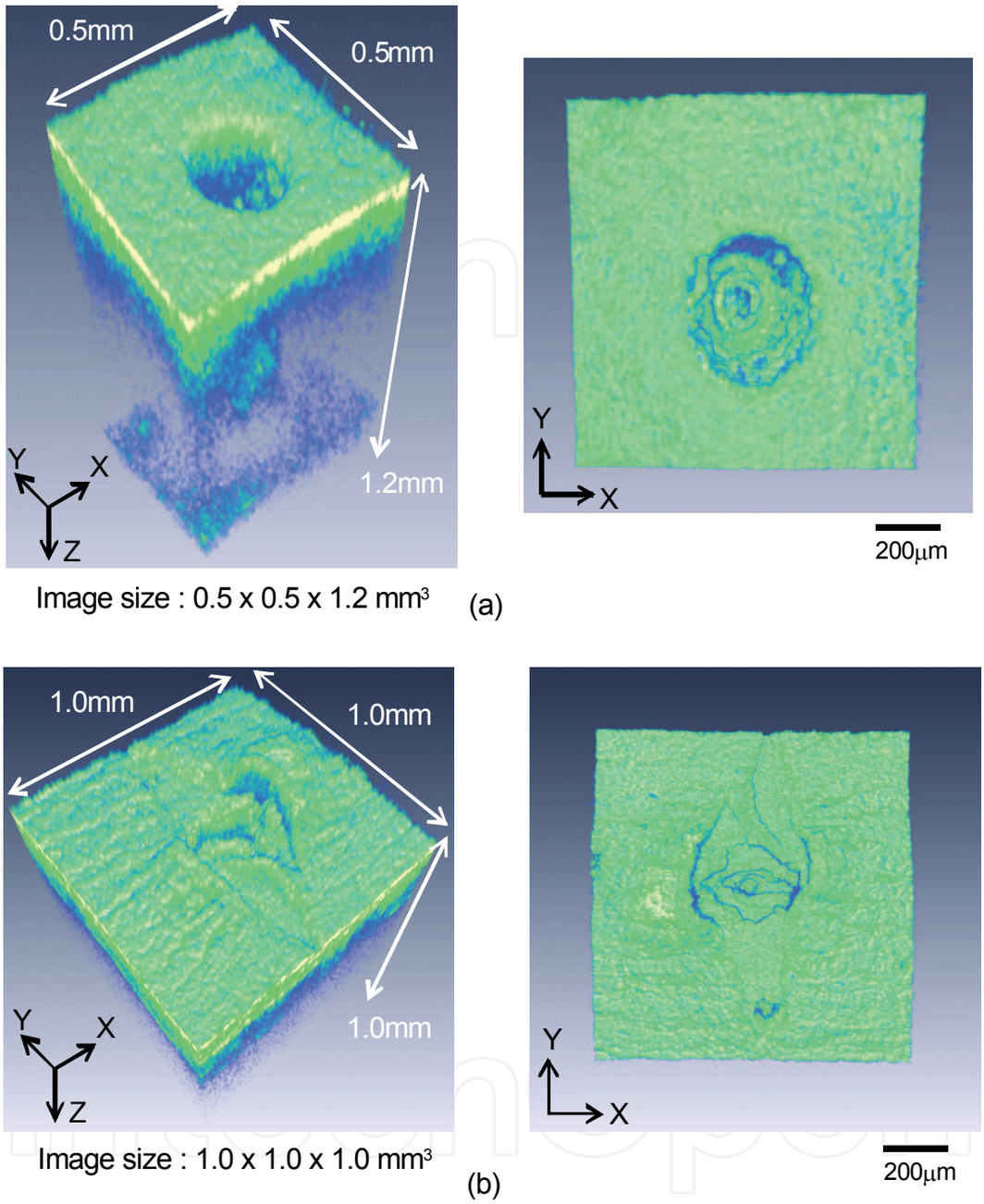

Fig. 11. 3D-OCT images of ablation crater. (a) dog aorta, (b) human tooth.

4. Discussion and conclusion

We have demonstrated the laser ablation system with a function of in-situ OCT observation of biological-tissue surface. In the experiment, time-serial OCT images of craters were carried out, and then the depth of the crater of tissue and the ablation rate were determined. Furthermore, dynamic analysis of tissue laser ablation has been demonstrated based on real-time OCT imaging of craters for both hard and soft tissues. In a human tooth, time variation

of the crater depth can be measured very precisely with a standard deviation comparable to the coherence length of the SS-OCT. This results in a determination of the ablation rate with an accuracy below 0.01 μm / pulse.

At the interface between the enamel and the dentine, the ablation rate changes drastically, as does the crater shape, because of the difference in hardness between these two media. The higher ablation rate causes a narrower crater, and vice versa. The volume ablation rate increase can be evaluated from the OCT images of the crater and is in linear proportion to the input laser fluence. On the other hand, during laser ablation of soft tissue, such as the aorta of a dog, thermal deformation of the crater is found, including upheaval and removal of tissues. Thus, real-time OCT imaging is thus very useful for dynamic analysis of tissue laser ablation.

In the present fusion system of laser ablation and OCT, the image resolution is not yet sufficiently low for dynamic analysis of tissue ablation. The image resolution should be a few microns or less to allow monitoring of tissue treatment at the size of a cell. In this case, the focal depth of an objective becomes a few tens of microns, and proper focus tracking is then required for clear OCT imaging during tissue laser ablation.

5. References

Trokel, S. L.; Srinivasan, R. & Braren, B. (1983). Excimer laser surgery of the cornea. *American Journal of Ophthalmology* 96, 710-715.

Puliafito, C.A.; Steinnert, R. F.; Deeutsch, T. F.; Hillenkamp,F.; Dehm, E. J. & and Adler, C. M. (1985). Excimer laser ablation of the cornea and lens. *Ophthalmology* 92, 741-748.

Isner, J.M.; Steg, P. G. & Clarke, R. H.(1987). Current status of car- diovascular laser therapy. *IEEE Journal of Quantum Electronics* 23, 1756-1771.

Esenaliev, R. A.; Oraevsky, S.; Rastergar, C. Frederickson and M. Motamedi. Mechanism of dye-enhanced pulsed laser ablation of hard tissues: implications for dentistry. *IEEE Journal of Selected Topics in Quantum Electronics* 2, 836-846.

Huang D.; Swanson E. A., Lin C. P.; Schuman J. S.; Stinson W. G.; Chang W.; Hee M. R.; Flotte T.; Gregory K.; Puliafito C. A. & Fujimoto J. G. (1991). Optical coherence tomography. Science 254, 1178-1181.

Hee M. R.; Izatt J. A.; Swanson E. A.; Huang D.; Schuman J. S.; Lin C. P.; Puliafito C. A. & Fujimoto J. G. (1995). Optical coherence tomography of the human retina. (1995). Arch. *Ophthalmology* 113, 325-332.

Izatt, J.A.; Kulkarni, M. D.; Wang, H. D.; Kobayashi, K. & Sivak, M. V. (1996). Optical coherence tomography and microscopy in gastrointestinal tissues. *IEEE Journal of Selected Topics in Quantum Electronics* 2, 1017-1028, 1996.

Brezinski, M.E.; Tearney, G. J.; Bouma, B. E.; Izatt, J. A.; Hee, M. R.; Swanson, E. A.; Southern, J. F. & Fujimoto, J. G. (1996). Optical coherence tomography for optical biopsy. Properties and demonstration of vascular pathology.*Circulation* 93, 1206-1213.

Boppart, S. A.; Herrmann, J.; Pitris, C.; Stamper, D. L.; Brezinski, M. E. & Fujimoto, J. G. (1999). High-resolution optical coherence tomography-guided laser ablation of surgical tissue. *J Surg. Res.* 82, 275-284.

Alfredo, D. R.; Anupama, V. S.; Charles, Q. L.; Robert, S. J. & Daniel, F. (2004). Peripheral thermal and mechanical damage to dentin with microsecond and sub-microsecond 9.6 μm, 2.79 μm, and 0.355 μm laser pulses. *Lasers Surg. Med.* 35, 214-228.

Haruna ,M.; Konoshita, R.; Ohmi, M.; Kunizawa , N. & Miyachi, M. (2001). In-situ tomographic observation of tissue surface during laser ablation, *Proc. SPIE* 4257, 329-333.

Ohmi, M.; Tanizawa, M., Fukunaga, A. & Haruna, M. (2005). In-situ observation of tissue laser ablation using optical coherence tomography. *Opt. Quantum. Electron.* 37, 1175-1183.

Ohmi, M.; Nishino, M.; Ohnishi, M.; Hashishin, Y. & Haruna ,M. (2007). An approach to high-resolution OCT analyzer for laser ablation of biological tissue. *Proc. 3rd Asian and Pacific Rim Symp. Biophotonics (APBP2007) (Cairns)* 99-100.

Yun, S.; Tearney, G.; de Bore, J. F.; Iftimia, N. & Bouma, B. E. (2003). High speed optical frequency-domain imaging. *Opt . Express* 11, 2953-2963.

de Bore, J. F.; Cense,B.; Park, B. H.; Pierce, M. C., Tearney, G. J. & Bouma, B. E. (2003). Improved signal-to-noise ratio in spectral-domain compared with time-domain optical coherence tomography. *Opt.Lett.* 28, 2067-2069.

Ohmi, M.; Ohnishi, M.; Takada, D. & Haruna, M. (2010). Dynamic analysis of laser ablation of biological tissue using real-time optical coherence tomography. *Meas. Sci. Tecnol.* 21, 094030.

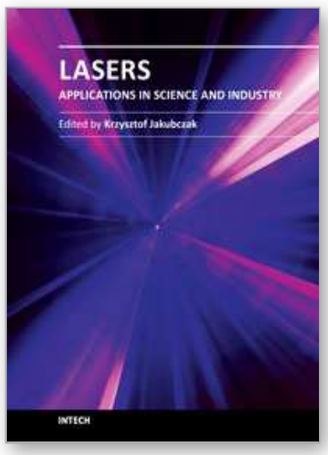

Lasers - Applications in Science and Industry
Edited by Dr Krzysztof Jakubczak

ISBN 978-953-307-755-0
Hard cover, 276 pages
Publisher InTech
Published online 09, December, 2011
Published in print edition December, 2011

The book starts with basic overview of physical phenomena on laser-matter interaction. Then it is followed by presentation of a number of laser applications in the nano-particles and thin films production, materials examination for industry, biological applications (in-vitro fertilization,tissue ablation) and long-range detection issues by LIDARs.

How to reference
In order to correctly reference this scholarly work, feel free to copy and paste the following:

Masato Ohmi and Masamitsu Haruna (2011). Dynamic Analysis of Laser Ablation of Biological Tissue by Optical Coherence Tomography, Lasers - Applications in Science and Industry, Dr Krzysztof Jakubczak (Ed.), ISBN: 978-953-307-755-0, InTech, Available from: http://www.intechopen.com/books/lasers-applications-in-science-and-industry/dynamic-analysis-of-laser-ablation-of-biological-tissue-by-optical-coherence-tomography

INTECH
open science | open minds

InTech Europe
University Campus STeP Ri
Slavka Krautzeka 83/A
51000 Rijeka, Croatia
Phone: +385 (51) 770 447
Fax: +385 (51) 686 166
www.intechopen.com

InTech China
Unit 405, Office Block, Hotel Equatorial Shanghai
No.65, Yan An Road (West), Shanghai, 200040, China
中国上海市延安西路65号上海国际贵都大饭店办公楼405单元
Phone: +86-21-62489820
Fax: +86-21-62489821

IntechOpen